Engineering Journal issn: 0125-8281

Article

Modeling of Partial Hydrogenation of Polyunsaturated Fatty Acid Methyl Esters in a Trickle Bed Reactor

Yuswan Muharam[a,*], Taqi Aufa[b], and Teguh Budi Santoso[c]

Department of Chemical Engineering, Faculty of Engineering, University of Indonesia, Kampus Baru UI Depok 16424, West Java, Indonesia
E-mail: [a]muharam@che.ui.ac.id (Corresponding author), [b]taqiaufa@hotmail.com, [c]teguh.bs@yahoo.com

Abstract. Partial hydrogenation of polyunsaturated fatty acid methyl esters in a trickle-bed reactor was modeled and simulated in this study with the objectives being to investigate the performance of the reactor, to predict the effect of process parameters on the reactor performance, and to observe the radial heat transfer in the reactor. The reactor possessed the aspect ratio of 100 and was packed with spherical catalyst particles. A steady-state heterogeneous model was applied. The gas and liquid phases were modeled in two-dimensional axisymmetric model, which consist of mass balance for each phase, energy balance and momentum balance. The momentum balance was based on the Darcy equation for two fluid phases passing through porous media. Mixing in both fluid phases is also described by dispersion coefficients. The three-dimensional solid phase model considered diffusive transport in the catalyst pores and surface reactions. Methyl linoleate was considered as polyunsaturated fatty acid methyl ester representative, and cis-methyl oleate, trans-methyl oleate and methyl stearate were as the hydrogenated fatty acid methyl esters. The simulation results for the inlet temperature of 433 K and the reactor pressure of 611 kPa with the gas flowrate being 43 times higher than the liquid one shows that the process reached 78.22% methyl linoleate conversion. The concentrations of cis-methyl oleate, trans-methyl oleate and methyl stearate at the reactor outlet are 16.2 mol/m^3, 17.4 mol/m^3 dan 16.6 mol/m^3, respectively. The total methyl oleate produced is about twice that of methyl stearate, and its selectivity is about 53%.

Keywords: H-FAME, mathematical modeling, partial hydrogenation, trickle-bed reactor, upgrading.

ENGINEERING JOURNAL Volume 24 Issue 4
Received 5 December 2019
Accepted 21 April 2020
Published 31 July 2020
Online at https://engj.org/
DOI:10.4186/ej.2020.24.4.195

This article is based on the presentation at The 4th International Tropical Renewable Energy Conference (i-TREC 2019) in Bali, Indonesia, 14 - 16 August 2019.

DOI:10.4186/ej.2020.24.4.195

1. Introduction

The energy crisis, the strict law on automotive pollutants and the dependence on imported petroleum crude cause alternative fuels to be widely used in many countries. Biodiesel as an alternative fuel has been used as a mixture with diesel fuel in unmodified diesel engines. That is because biodiesel has the similar properties with diesel without a significant reduction in engine performance despite the higher fuel consumption due to its lower heating value [1].

Biodiesel or fatty acid methyl ester (FAME) has advantages over diesel in terms of biodegradable, non-toxic, higher cetane number, higher flash point [2,3] and better lubrication property [4-6]. Exhaust emission including CO, hydrocarbon and particulate matters significantly reduce while NO emission increases [7-8].

In spite of having the exceptional advantages above, biodiesel possesses several disadvantages, i.e. oxidative susceptibility to ambient air oxygen, lower temperature performance and higher NO emission [9,10,11]. Because of the low oxidation stability property, the quantity of biodiesel that can be mixed with diesel is limited. This property is the result of double bonds in polyunsaturated molecules in biodiesel which are easily oxidized [10,11]. Polyunsaturated FAME is more susceptible to oxidation than monounsaturated FAME, and monounsaturated FAME is more susceptible to oxidation than saturated FAME. However, the cold flow properties decrease in reverse order [10-13]. As a result, monounsaturated FAME is a valuable component for high-quality biodiesel with the good oxidation stability and cold flow properties [14,15].

The partial hydrogenation of polyunsaturated fatty acid methyl esters can improve the quality of biodiesel. This process intends to convert polyunsaturated FAME into monounsaturated FAME (C18:1) while suppressing the formation of saturated FAME [16-17]. Several studies have tried to adjust the oxidation stability and the cold flow properties of biodiesel through the partial hydrogenation of polyunsaturated FAME to monounsaturated FAME with supported transition metal catalysts, i.e. Ni, Cu, Rh and Pd [15, 18]. Partially hydrogenated fatty methyl esters or so-called H-FAME to increase the oxidation stability without the influence on the cold flow properties have been obtained.

In addition to the hydrogenation catalyst, the hydrogenation reactor also affects the reactant conversion and the product selectivity in the partial hydrogenation of polyunsaturated fatty acid methyl esters. Two types of reactors are used for this reaction, i.e. stirred batch reactors and trickle-bed reactors. In a stirred batch reactor, the hydrogenation catalyst is mixed with liquid FAME by a rotating impeller and the rising bubbles of hydrogen from the bottom of the reactor are sucked into the low-pressure liquid behind the impeller blades to then disperse into the bulk liquid. However, the catalyst lifetime due to mechanical damage reduces [19, 20]. This catalyst reduction also causes several problems in the ability of hydrogenated product filters. In a trickle-bed reactor, the gas and liquid phases move continuously in co-current flow mode through a high-pressure bed [21, 22]. During the partial hydrogenation process, hydrogen transports from the gas phase to the liquid phase and reacts with FAME to produce H-FAME. Trickle-bed reactors are generally characterized by high pressure drops and low catalyst loss. There are no moving parts in this type of reactor so the separation of catalysts and products is easy and the maintenance cost is relatively lower. Another advantage is that it reduces mechanical damage to catalyst particles, but on the other hand, problems such as catalyst deactivation are also a main characteristic of this reactor [23].

The partial hydrogenation of polyunsaturated FAME in a stirred batch reactor and a trickle-bed reactor gives different results. The partial hydrogenation of polyunsaturated FAMEs in a stirred batch reactor provides a higher selectivity towards C18:1 than that of a trickle-bed reactor. However, at the low conversion (78%), the selectivity of C18:1 obtained from both types of reactors were almost the same [24].

Trickle-bed reactors often show unacceptable levels of performance when upgraded from laboratory reactors to commercial reactors [25]. Most of the reduced performance or inefficiency of the reactor on a large scale comes from the maldistribution of gas/liquid flow and the difficult control of temperature. Other factors such as the operating temperature and pressure, the gas and liquid flow rates and the size of the reactor and catalyst also affect the performance of trickle-bed reactors.

Many attempts were made to understand various aspects of the performance of this trickle-bed reactor using numerical methods. The present study investigated the performance of the partial hydrogenation of FAME in a trickle bed reactor through mathematical modeling and numerical simulation, predicted the effect of the process parameters on the reactor performance, and observed the radial heat transfer in the reactor.

2. Modeling

Trickle-bed reactor is a type of three-phase fixed-bed reactor, as shown in Fig. 1. This reactor is packaged with catalyst spheres or pellets. For the partial hydrogenation of polyunsaturated FAME to H-FAME the gaseous hydrogen and the liquid FAME enter continuously from the top of the reactor. Inside the reactor the two fluids flow co-current through the bed interstice where the liquid flows in a thin gentle stream. As the gas and the liquid are in intimate contact, hydrogen transports to the liquid phase by traversing the gas-liquid interphase. Furthermore, dissolved hydrogen and FAME enter the catalyst pores by crossing the liquid-solid interphase. Dissolved hydrogen and FAME diffuse in the catalyst pores before they are adsorbed onto the catalyst surface in the pore walls and react to yield products. The models used in this study are phenomenological model coupling transport theories and chemical reactions. The models consist of two parts: those for physical transport in the reactor bed interslice and those in the catalyst particles.

Fig. 1. Trickle-bed reactor.

The models for physical transport in the reactor bed interslice are two-dimensional axisymmetric models, and those for the catalyst particles are three-dimensional spherical models.

In order to reduce the computing loads without significantly changing simulation results, the following assumptions were appointed:

- The system is steady state.
- The momentum balance is approached by two-phase Darcy equations.
- The fluid mixing in the reactor bed occurs through dispersion and convection mechanisms.
- The gas and liquid saturations in adjacent zones to the reactor inlet are uniform.
- The gas is ideal.
- The catalyst particles are perfectly spherical and uniformly distributed.
- Catalyst deactivation is ignored.
- The catalyst particles are fully wetted by liquid.
- Biodiesel is represented by a mixture of methyl linoleate (polyunsaturated FAME), cis-methyl oleate and trans-methyl oleate (monounsaturated FAME) as well as methyl stearate (saturated FAME).
- The temperature is in locally thermal equilibrium.
- The foaming phenomenon is ignored.
- The heat transfer rate from the reactor wall to the cooling media is much faster than that from the reactor bed to the reactor wall and is therefore ignored.

2.1. Mass Transfer

The mass transfers occur in the gas phase for hydrogen and in the liquid and solid phases for dissolved hydrogen, methyl linoleate, methyl oleate and methyl stearate.

The mass transfer in the gas phase is described in Eq. (1):

$$\frac{D_{\mathrm{G}r}}{r}\frac{\partial}{\partial r}\left(r\frac{\partial C_{\mathrm{H_2,G}}}{\partial r}\right)+D_{\mathrm{G}z}\frac{\partial^2 C_{\mathrm{H_2,G}}}{\partial z^2}-u_{\mathrm{G}r}\frac{\partial C_{\mathrm{H_2,G}}}{\partial r} \quad (1)$$

$$-u_{\mathrm{G}z}\frac{\partial C_{\mathrm{H_2,G}}}{\partial z}-k_{\mathrm{GL,H_2}}a\left(\frac{p_{\mathrm{H_2}}}{RTH_i}-C_{\mathrm{H_2,L}}\right)=0$$

The mass transfer in the liquid phase is explained in Eq. (2) and Eq. (3):

$$\begin{aligned}&\frac{D_{\mathrm{L}r}}{r}\frac{\partial}{\partial r}\left(r\frac{\partial C_{\mathrm{H_2,L}}}{\partial r}\right)+D_{\mathrm{L}z}\frac{\partial^2 C_{\mathrm{H_2,L}}}{\partial z^2}-u_{\mathrm{L}r}\frac{\partial C_{\mathrm{H_2,L}}}{\partial r}\\&-u_{\mathrm{L}z}\frac{\partial C_{\mathrm{H_2,L}}}{\partial z}+k_{\mathrm{GL,H_2}}a\left(\frac{p_{\mathrm{H_2}}}{RTH_i}-C_{\mathrm{H_2,L}}\right)\\&-k_{\mathrm{LS,H_2}}a\left(C_{\mathrm{H_2,L}}-C_{\mathrm{H_2,S}}\right)=0\end{aligned} \quad (2)$$

$$\begin{aligned}&\frac{D_{\mathrm{L}r}}{r}\frac{\partial}{\partial r}\left(r\frac{\partial C_{i,\mathrm{L}}}{\partial r}\right)+D_{\mathrm{L}z}\frac{\partial^2 C_{i,\mathrm{L}}}{\partial z^2}-u_{\mathrm{L}r}\frac{\partial C_{i,\mathrm{L}}}{\partial r}\\&-u_{\mathrm{L}z}\frac{\partial C_{C_{i,\mathrm{L}}}}{\partial z}-k_{\mathrm{LS,H_2}}a_{\mathrm{S}}\left(C_{i,\mathrm{L}}-C_{i,\mathrm{S}}\right)=0\end{aligned} \quad (3)$$

The mass transfer in the catalyst particles is explained in Eq. (4):

$$\frac{D_{\mathrm{eff},i}}{r_{\mathrm{s}}^2}\frac{\partial}{\partial r_{\mathrm{s}}}\left(r_{\mathrm{s}}^2\frac{\partial C_{i,\mathrm{S}}}{\partial r_{\mathrm{s}}}\right)-R_i=0 \quad (4)$$

where $C_{\mathrm{H_2,G}}$ and $C_{\mathrm{H_2,L}}$ are the hydrogen concentrations in the gas and liquid phases, $C_{i,\mathrm{L}}$ is the FAME component concentrations in the liquid phases, $C_{i,\mathrm{S}}$ are the hydrogen and FAME component concentrations in the catalyst particles, $D_{\mathrm{G}r}$ and $D_{\mathrm{G}z}$ are the radial and axial gas dispersion coefficients, $D_{\mathrm{L}r}$ and $D_{\mathrm{L}z}$ are the radial and axial liquid dispersion coefficients, $u_{\mathrm{G}r}$ and $u_{\mathrm{G}z}$ are the radial and axial gas velocities, $u_{\mathrm{L}r}$ and $u_{\mathrm{L}z}$ are the radial and axial liquid velocities, $k_{\mathrm{GL,H_2}}$ and $k_{\mathrm{LS,H_2}}$ are the hydrogen mass transfer coefficients through the gas-liquid and liquid-solid interphases, $k_{\mathrm{GL},i}$ and $k_{\mathrm{LS},i}$ are the FAME component mass transfer coefficients through the gas-liquid and liquid-solid interphases, a is the gas-liquid interphase specific surface area, a_{S} is the liquid-solid interphase specific surface area, $p_{\mathrm{H_2}}$ is the hydrogen partial pressure, H_i is the Henry's constant of hydrogen, $D_{\mathrm{eff},i}$ is the *i*-component effective diffusivity, and R_i is the *i*-component chemical reaction rates. The chemical reaction kinetics were developed by Cabrera and Grau using Ni/αAl_2O_3 catalyst [26].

The gas-liquid mass transfer coefficient is taken from the Sherwood number developed by Goto and Smith [27]:

$$Sh_{\mathrm{GL}}=\frac{k_{\mathrm{GL},i}a}{D_{\mathrm{L},i}}=6\left(\frac{G_{\mathrm{L}}}{\mu_{\mathrm{L}}}\right)^{0.41}\left(\frac{\mu_{\mathrm{L}}}{\rho_{\mathrm{L}}D_{\mathrm{L},i}}\right)^{0.5} \quad (5)$$

where $D_{\mathrm{L},i}$ is the diffusion coefficient of *i*-component, μ_{L} is the liquid viscosity of *i*-component, ρ_{L} is the liquid density of *i*-component and G_{L} is the Galileo number.

The coefficient of mass transfer from the liquid phase to the solid phase is predicted using the Sherwood number proposed by Van Krevelen and Krekels [28]:

$$Sh_{\mathrm{LS}}=\frac{k_{\mathrm{LS},i}a_{\mathrm{S}}}{D_{\mathrm{L},i}}=1.8\left(\frac{G_{\mathrm{L}}}{\mu_{\mathrm{L}}}\right)^{0.5}\left(\frac{\mu_{\mathrm{L}}}{\rho_{\mathrm{L}}D_{\mathrm{L},i}}\right)^{1/3} \quad (6)$$

2.2. Energy Transfer

The governing equation for the energy transfer is:

$$\frac{k_{\mathrm{eff},r}}{r}\frac{\partial}{\partial r}\left(r\frac{\partial T}{\partial r}\right)+k_{\mathrm{eff},z}\frac{\partial^2 T}{\partial z^2} -\rho_{\mathrm{f}}C_{\mathrm{p,f}}\left(u_r\frac{\partial T}{\partial r}+u_z\frac{\partial T}{\partial z}\right)+Q=0 \tag{7}$$

where T is the temperature, ρ_{f} is the mixed fluid density, $C_{\mathrm{p,f}}$ is the mixed fluid heat capacity, u_r and u_z are the radial and axial average velocities and Q is the reaction heat.

The axial effective thermal conductivity is calculated using the following equation:

$$k_{\mathrm{eff},z}=\left(1-\varepsilon_{\mathrm{p}}\right)k_{\mathrm{S}}+\varepsilon_{\mathrm{L}}k_{\mathrm{L}}+\varepsilon_{\mathrm{G}}k_{\mathrm{G}} \tag{8}$$

where ε_{p} is the bed porosity, ε_{L} and ε_{G} are the liquid and gas holdups, k_{G}, k_{L} and k_{S} are the gas, liquid and solid thermal conductivities.

The radial effective thermal conductivity is calculated using the equation proposed by Taulamet et. al. [29]:

$$k_{\mathrm{eff},r}=k_{\mathrm{e0}}+0.104\left(\frac{L}{\beta_{\mathrm{L}}}\right)d_{\mathrm{p}}Cp_{\mathrm{eff}} \tag{9}$$

where k_{e0} is the conduction contribution factor, d_{p} is the catalyst diameter and β_{L} is the total liquid saturation.

The effective heat capacity is calculated using the following equation:

$$Cp_{\mathrm{eff}}=(1-\varepsilon_{\mathrm{P}})\rho_{\mathrm{S}}Cp_{\mathrm{S}}+\varepsilon_{\mathrm{L}}\rho_{\mathrm{L}}Cp_{\mathrm{L}}+\varepsilon_{\mathrm{G}}k_{\mathrm{G}} \tag{10}$$

where Cp_{S} and Cp_{L} are the solid and liquid heat capacities, d_{p} is the catalyst diameter and β_{L} is the total liquid saturation.

2.3. Momentum Transfer

The mixture continuity equation is

$$\frac{1}{r}\frac{\partial(ru_r)}{\partial r}+\frac{\partial(\rho u_z)}{\partial z}=0 \tag{11}$$

The mass conservation equation of phase 1 (liquid) is

$$\frac{1}{r}\frac{\partial(rc_{\mathrm{L}}u_r)}{\partial r}+\frac{\partial(c_{\mathrm{L}}u_z)}{\partial z}=\frac{1}{r}\frac{\partial}{\partial r}\left(rD_{\mathrm{c}}\frac{\partial c_{\mathrm{L}}}{\partial r}\right)+\frac{\partial}{\partial z}\left(D_{\mathrm{c}}\frac{\partial c_{\mathrm{L}}}{\partial z}\right) \tag{12}$$

where c_{L} is the liquid fluid content ($=\rho_{\mathrm{L}}s_{\mathrm{L}}$) and s_{L} is the liquid saturation ($=\varepsilon_{\mathrm{L}}/\varepsilon_{\mathrm{p}}$).

The capillary diffusion coefficient is a function of capillary pressure expressed as

$$D_{\mathrm{c}}=\frac{\kappa_{r\mathrm{L}}\kappa}{\mu_{\mathrm{L}}}(s_{\mathrm{L}}-1)\frac{\partial p_{\mathrm{c}}}{\partial s_{\mathrm{L}}} \tag{13}$$

where p_{c} is the capillary pressure which is the difference between the gas and liquid pressures.

The gas saturation is calculated by Eq. (14):

$$s_{\mathrm{G}}=1-s_{\mathrm{L}} \tag{14}$$

The bed permeability is calculated using the modified Ergun equation as proposed by Propp et al. [30]:

$$\kappa=\left(\frac{180\left(1-\varepsilon_{\mathrm{p}}\right)^2}{d_{\mathrm{p}}^2\varepsilon_{\mathrm{p}}^3}+\frac{1.8\left(1-\varepsilon_{\mathrm{p}}\right)\rho U_0}{\mu d_{\mathrm{p}}\varepsilon_{\mathrm{p}}^3}\right)^{-1} \tag{15}$$

where U_0 is the inlet mixed superficial velocity.

The relative permeability of each phase is the comparison of the absolute permeability of the phase to the porous material permeability and expressed by [31]:

$$\kappa_{r\mathrm{L}}=\delta_{\mathrm{L}}^{2.43} \tag{16}$$

$$\kappa_{r\mathrm{G}}=s_{\mathrm{G}}^{4.80} \tag{17}$$

where δ_{L} is liquid reduced saturation.

The relationship between the velocity vectors and the pressure is as follows:

$$u_r=-\frac{\kappa}{\mu}\frac{\partial p}{\partial r} \tag{18}$$

and

$$u_z=-\frac{\kappa}{\mu}\frac{\partial p}{\partial z} \tag{19}$$

2.4. Boundary Conditions

The change equations above are solved numerically using boundary conditions.

At the reactor inlet:

$$\begin{gathered} -D_{\mathrm{G},i}\frac{\partial C_{\mathrm{G},i}}{\partial z}+u_{\mathrm{G}z}C_{\mathrm{G},i}=U_{\mathrm{G0}}C_{\mathrm{G0}} \\ -D_{\mathrm{L},i}\frac{\partial C_{\mathrm{L},i}}{\partial z}+u_{\mathrm{L}z}C_{\mathrm{L},i}=U_{\mathrm{L0}}C_{\mathrm{L0}} \\ -k_{\mathrm{eff},z}\frac{\partial T}{\partial z}+\rho_{\mathrm{f}}C_{\mathrm{p,f}}u_{\mathrm{L}z}T=\rho_{\mathrm{f}}C_{\mathrm{p,f}}U_{\mathrm{L0}}T_0 \\ \rho u_z=(s_{\mathrm{L}}\rho_{\mathrm{L}}+s_{\mathrm{G}}\rho_{\mathrm{G}})U_0 \end{gathered} \tag{20}$$

At the reactor outlet:

$$\begin{gathered} D_{\mathrm{G},i}\frac{\partial C_{\mathrm{G},i}}{\partial z}=0 \qquad D_{\mathrm{L},i}\frac{\partial C_{\mathrm{L},i}}{\partial z}=0 \\ k_{\mathrm{eff},z}\frac{\partial T}{\partial z}=0 \qquad D_{\mathrm{c}}\frac{\partial c_{\mathrm{L}}}{\partial z}=0 \end{gathered} \tag{21}$$

At the reactor centerline:

$$\begin{gathered} \frac{\partial C_{\mathrm{G},i}}{\partial r}=0 \qquad \frac{\partial C_{\mathrm{L},i}}{\partial r}=0 \\ \frac{\partial T}{\partial r}=0 \qquad \rho u_r=0 \end{gathered} \tag{22}$$

At the reactor walls:

$$\begin{gathered} \frac{\partial C_{\mathrm{G},i}}{\partial r}=0 \qquad \frac{\partial C_{\mathrm{L},i}}{\partial r}=0 \\ -k_{\mathrm{eff},r}\frac{\partial T}{\partial r}=h(T-T_{\mathrm{w}}) \qquad \rho u_r=0 \end{gathered} \tag{23}$$

where T_w is the reactor wall temperature and h is the bed-wall heat transfer coefficient, which is formulated according to Taulamet et al. [29]:

$$Nu = \frac{hd_P}{k_{eff,r}} = 2.51\left[1 - \exp\left(-\frac{4.71d_P}{d_R}\right)\right] Re_L^{0.68} \quad (24)$$

where Nu is the Nusselt number, d_R is the reactor diameter, and Re_L is the fluid Reynold number.

At the external surface of catalyst sphere:

$$-D_{eff,i}\frac{\partial C_{i,S}}{\partial r_s} = k_{LS,H_2} a_S (C_{i,L} - C_{i,S}) \quad (25)$$

At the symmetry point of catalyst sphere:

$$\frac{\partial C_{i,S}}{\partial r_s} = 0 \quad (26)$$

3. Results and Discussion

All the above changing equations and their boundary conditions were numerically solved using COMSOL Multiphysics. The simulation was performed by specifying the process and geometric parameters as shown in Table 1.

Figure 2 shows the calculated profiles of the concentrations of methyl linoleate, *cis*-methyl oleate, *trans*-methyl oleate and methyl stearate in the liquid phase. From the figure it can be seen that there are significant changes in the concentrations of the reactants and the products along the reactor. Pure methyl linoleate of 62.6 mol/m^3 fed into the reactor was converted by chemical reactions along the reactor, leaving 13.7 mol/m^3 in the outlet of the reactor. This is equivalent to the conversion of about 78%. The products exiting the reactor have comparable concentrations, which indicates that the competition between products occurs. The concentrations of *cis*-methyl oleate, *trans*-methyl oleate and methyl stearate at the reactor outlet are 16.2 mol/m^3, 17.4 mol/m^3 dan 16.6 mol/m^3, respectively. The total methyl oleate produced is about twice that of methyl stearate, and its selectivity is about 53%.

The changes in the concentrations of all species in the radial direction are insignificant indicating that the radial mass dispersion in the liquid phase is considerable high.

Figure 3 shows the profile of the methyl linoleate conversion along the reactor at the radial position of 0.4 m form the centerline of the reactor. It can be seen in the figure that the conversion increases along the reactor with a diminished gradient toward the reactor outlet. However, the conversion gradient is not yet flat near the outlet. This informs that the reactant conversion has not been maximized, and extending the reactor is an option that needs to be taken if the reactor performance is focused on the reactant conversion. If the purpose is to obtain a composition that provides high oxidative stability and high cold flow properties, the FAME composition at the reactor outlet needs to be considered as will be discussed later.

Table 1. The process and geometry parameters.

Parameter	Value
Inlet pressure	611 kPa
Inlet temperature	433 K
Cooling wall temperature	433 K
Reactor bed diameter	1.6 m
Reactor bed height	16 m
Catalyst particle diameter	1 mm
Inlet methyl linoleate	62.6 mol/m^3
Liquid flow rate	0.01921 m^3/s (7.5 kg/m^{2}s)
Gas flow rate	0.8339 m^3/s (0.14 kg/m^{2}s)
Flow direction	Co-current downflow

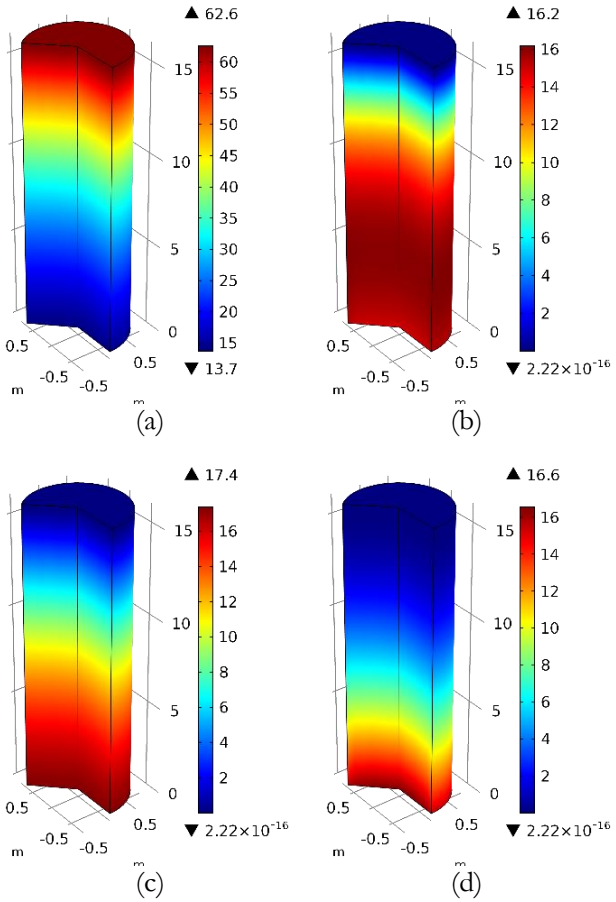

Fig. 2. The profiles of the concentrations of (a) methyl linoleate, (b) cis-methyl oleate, (c) trans-methyl oleate, (d) methyl stearate.

In the zone adjacent to the reactor inlet, the methyl linoleate reaction seems to be delayed, as can be seen from the flat curve of the conversion along that narrow zone. Since the model assumes that no hydrogen is dissolved at the inlet, the delay is caused by the lack of dissolved hydrogen in the narrow zone. In practice, FAME and hydrogen are premixed before entering the reactor. Thus, such a reaction delay is not expected to occur.

DOI:10.4186/ej.2020.24.4.195

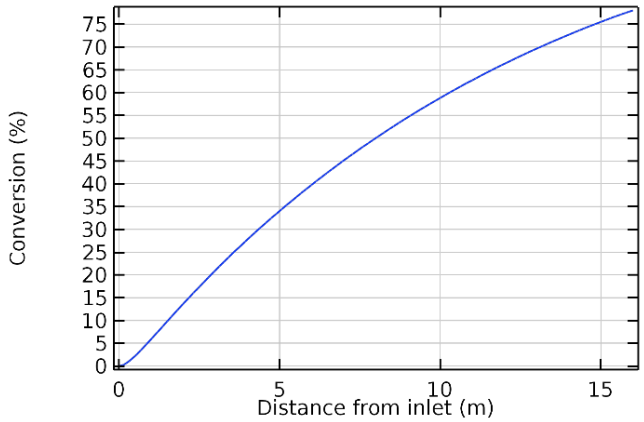

Fig. 3. The methyl linoleate conversion.

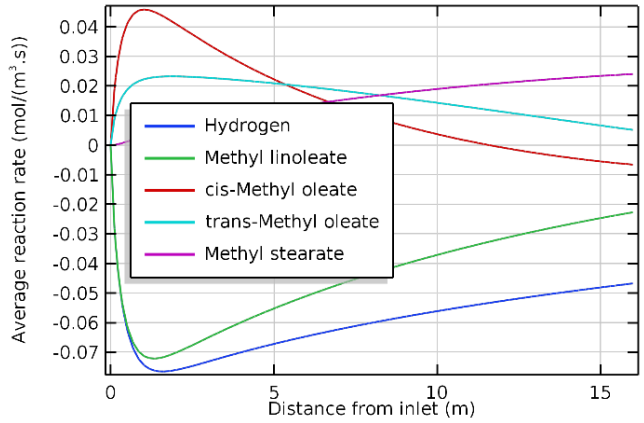

Fig. 4. The average chemical reaction rate.

Figure 4 shows the average reaction rates of dissolved hydrogen and FAME components along the reactor. The reaction rates of *cis*- and *trans*-methyl oleates increase along the first ninth of the reactor length, as a consequence of fast consumption rate of methyl linoleate throughout that position. This indicates that *cis*-methyl oleate is produced rather than consumed to become methyl stearate or isomerized to become *trans*-methyl oleate in this position. The highest reaction rate of *cis*-methyl oleate is approximately 0.05 mol/m^3.s, which takes place at about 1.5 m from the reactor inlet. At the same position the consumption rate of methyl linoleate is about -0.07 mol/m^3.s, which is its highest value.

The lowest reaction rate of hydrogenated FAME components in the first ninth of the reactor length is owned by methyl stearate. However, since methyl stearate is produced continuously from the partial hydrogenation of methyl oleates along the reactor without being consumed, its reaction rate is always positive.

The reaction rates of *cis*- and *trans*-methyl oleates decrease from the position of 1.5 m to the reactor outlet. It is understood that *cis* and *trans*-methyl oleates are the reactants for the formation of methyl stearate. *Cis* and *trans*-methyl oleates are the products of the methyl linoleate hydrogenation. At the same time, they are also hydrogenated to form methyl stearate, in addition to be isomerized. Since the concentration of methyl linoleate decrease towards the reactor outlet, the production rates of methyl oleates also decline. Conversely, since at the operating pressure of 611 kPa the dissolved hydrogen is adequately supplied to the liquid phase, the hydrogenation of methyl oleates continuously takes place. Despite the reaction rates of *cis*-methyl oleate and *trans*-methyl oleate decrease from the position of 1.5 m, as long as their values are positive, their production rate are still dominate than the consumption ones. The consumption rate of *cis*-methyl oleate equals the production one at the position of 12 m, which is marked by a zero-rate value. From this point to the reactor outlet, the consumption rate of *cis*-methyl oleate dominates the production rate. At the reactor outlet the reaction rate of *cis*-methyl oleate is around -0.0065 mol/m^3.s.

As for *trans*-methyl oleate, its reaction rate is always positive. Two possibilities occur: the consumption rate of *trans*-methyl oleate to produce methyl stearate is never higher than the production rate, or the isomerization always goes to *cis*-methyl oleate.

Figure 5(a) shows the temperature profiles in the axial direction. The partial hydrogenation of FAME is exothermic reactions with a low reaction enthalpy. The heat generated by the reactions only increases the temperature in the reactor to a maximum of 435 K, which is at the position adjacent to the reactor inlet, with the inlet and wall temperatures being 433 K. The temperature in the axial direction drops to 433 K at the position adjacent to the reactor outlet. The temperature at this position is the same as those at the feed and the reactor wall. This happens because the heat flux from the bed to the reactor wall increases along the reactor as can be seen in Fig. 5(b). At the position adjacent to the reactor outlet, the heat flux is 750 W/m^2.

Basically, the reactor wall acts more as a means to maintain the temperature inside reactor to be at around 433 K, rather than as a cooler. If the reactor wall is exposed to the atmosphere of 303 K in temperature, a decrease in temperature inside the reactor to below 433 K occurs. This leads to a lower conversion of methyl linoleate than that is discussed above.

Figure 6 exhibits the mass concentrations of methyl linoleate, total *cis*- and *trans*-methyl oleates and methyl stearate. The mass concentration was observed to determine the product compositions. It can be seen in the figure that the concentration of methyl oleates raises with the gradient being smaller downstream of the reactor. Similarly, the concentration of methyl stearate increases along the reactor. However, the increasing gradient of the concentration of methyl stearate escalates. This informs that the reactor length is very important to achieve the desired H-FAME mixture. As stated above, the best H-FAME is that with major methyl oleate and inconsiderable methyl linoleate to give a high oxidative stability and high cold flow properties. Despite it has the highest resistance to oxidation, methyl stearate is not desirable component. This is because it has a butter-like nature. Therefore, in order to realize H-FAME with the desired composition, it is necessary to properly design and operate its reactor.

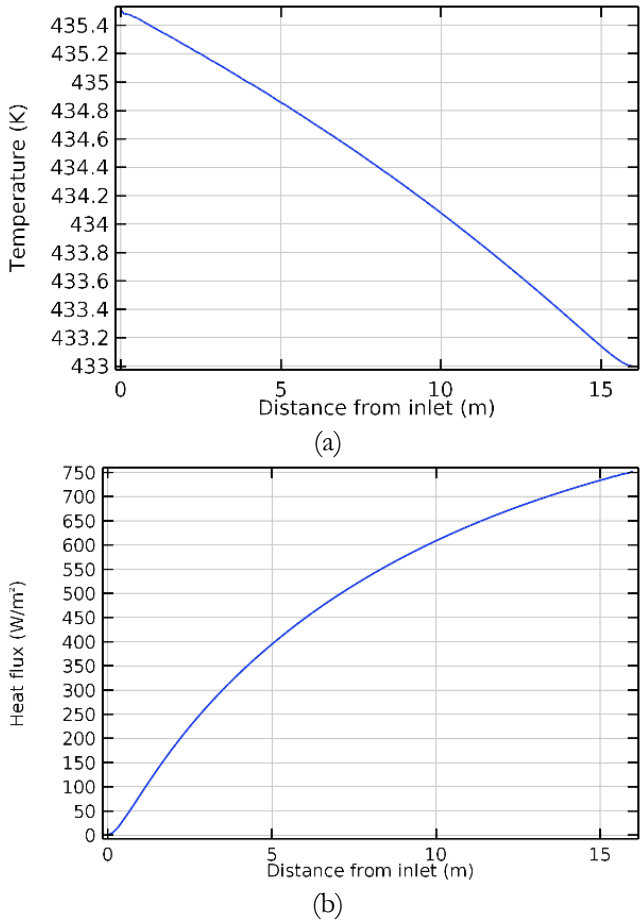

Fig. 5. The axial profiles of (a) the temperature, (b) the heat flux.

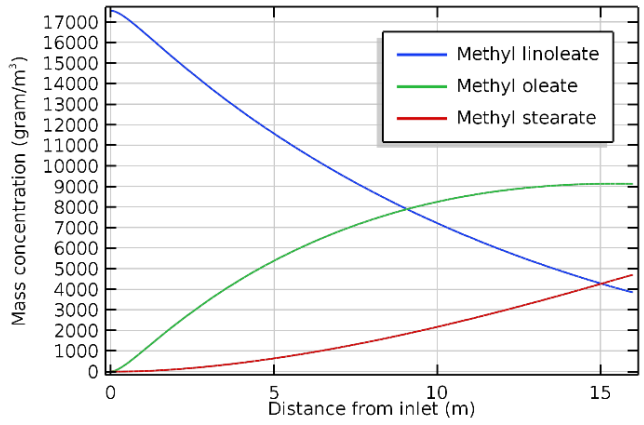

Fig. 6. The profiles of the mass concentrations of methyl linoleate, methyl oleate and methyl stearate.

The parameters that must be evaluated in designing and operating the reactor include the temperature and pressure, the gas and liquid flowrates as well as the catalyst and reactor size. In this study the effect of the inlet temperature, the operating pressure and the catalyst diameter will be evaluated.

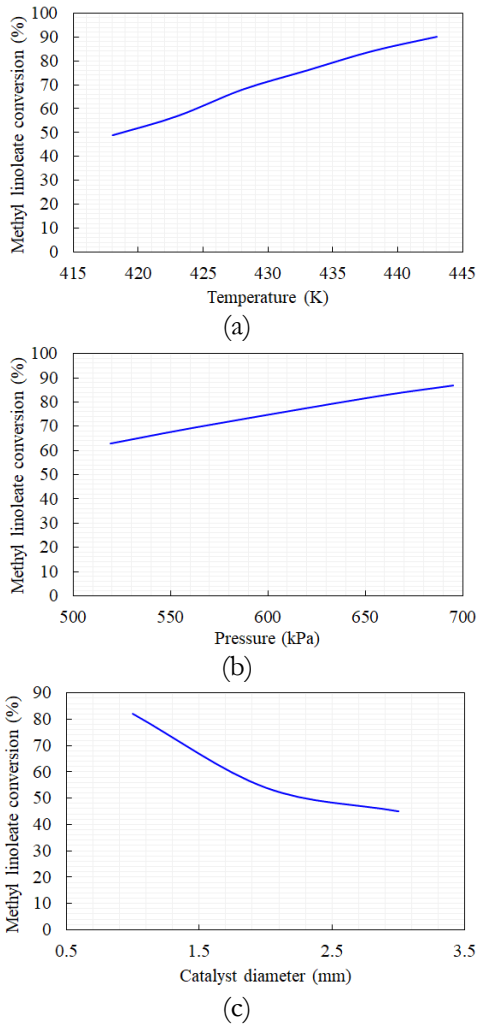

Fig. 7. Methyl linoleate conversion as a function of (a) inlet temperature, (b) pressure, (c) catalyst diameter

4. Sensitivity Analysis

Methyl linoleate and dissolved hydrogen are two reactants involved in the initiation reaction of the complex reactions of the hydrogenation process. They react on the catalyst surface providing sites for the reactant and product molecules in accordance with the surface mechanism described by Cabrera and Grau [26]. On the catalyst surface the reactant molecules collide producing the product molecules. This means that the reactant molecule atoms are redistributed in the product molecules. The reactant molecules must have enough kinetic energy so that the chemical bonds break during collisions and new bonds are formed. The factor affecting the kinetic energy of the reactant molecules is temperature. Then an increase in temperature can increase the number of collisions that result in bond breaking. This leads to the higher reaction rate and the higher reactant conversion. This is as shown in Fig. 7 (a). At 418 K, the methyl linoleate conversion is 49%. At 443 K, the methyl linoleate conversion is 90%, an increase of 84% from the conversion at 418 K. However, the resulting methyl oleate is lower than the methyl stearate at 443 K (6407 gram/m^3 to 9190 gram/m^3) as can be seen in Fig. 8. Such a composition is certainly not an expected result of the partial hydrogenation of polyunsaturated FAME.

DOI:10.4186/ej.2020.24.4.195

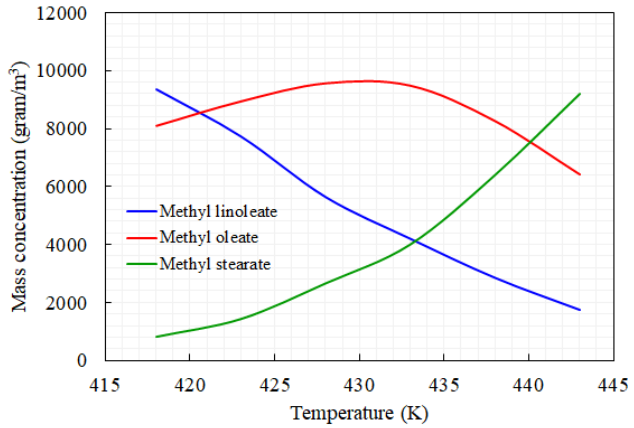

Fig. 8. The effect of the inlet temperature on the mass concentration of the products.

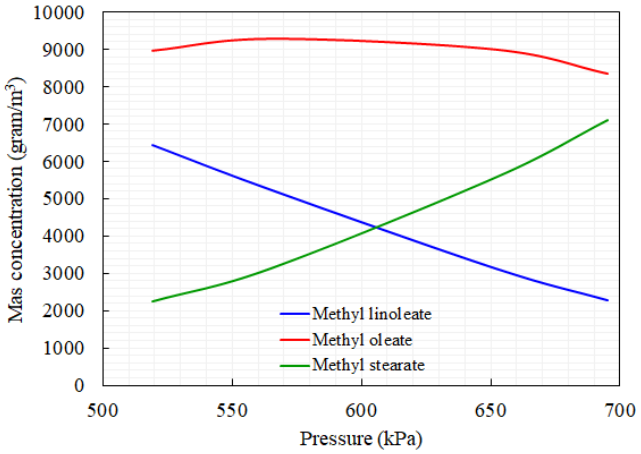

Fig. 9. The effect of the pressure on the mass concentration of the products.

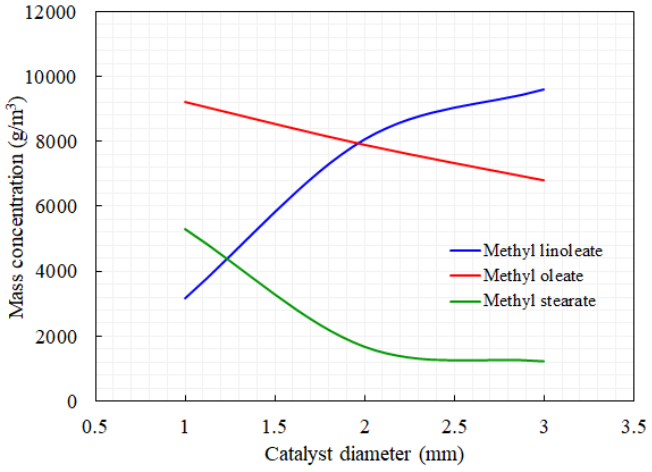

Fig. 10. The effect of the catalyst diameter on the mass concentration of the products.

The formation of methyl stearate increases exponentially with temperature over the simulated temperature range, whereas the formation of methyl oleate has a maximum value at 430 K. At that temperature, methyl oleate and methyl stearate formed are 9578 grams/m^3 and 2656 grams/m^3, and the remaining methyl linoleate is 5633 grams/m^3 with the conversion being 68%.

Pressure has an indirect effect on the chemical reaction rate of the liquid phase on the catalyst surface. The hydrogen pressure provides the hydrogen solubility in the liquid phase according to Henry's law of gas solubility in liquid. The higher pressure promotes more dissolved hydrogen. As a result, the hydrogen concentration available in the liquid phase to react with FAMEs is higher. This has an effect on the higher consumption rate of methyl linoleate so that the methyl linoleate conversion is also higher. The curve of the pressure effect on the methyl linoleate conversion is shown in Fig. 7 (b). It can be seen from the figure that the methyl linoleate conversion increases from 63% to 87% when the pressure rises from 519 kPa to 695 kPa. As can be seen in Fig. 9, the mass concentration of methyl oleate has a similar shape with that in Fig. 8, only it is rather flat. The highest value of the mass concentration of methyl oleate is 9296 grams/m^3, which takes place at 565 kPa. At the same pressure, the methyl stearate production is 3132 grams/m^3, whilst the remaining methyl linoleate is 5242 gram/m^3 with the conversion being 70%.

The catalyst diameter evaluated in this study ranges from 1 mm to 3 mm. The active sites of a metal are distributed in a porous support. The diameter of the catalyst sphere is related to the number of active sites accessed by the reactant molecules. Smaller diameters of the catalyst spheres make the reactant molecules to easily reach the active sites due to shorter passages of the pores. As a result, more reactant molecules cover the active sites, leading to higher reaction rate and higher reactant conversion. This phenomenon is shown by Fig. 7 (c). The catalyst of 3 mm in diameter gives the methyl linoleate conversion of 45%. The conversion increases to 82% when the catalyst diameter reduces to 1 mm. As can be seen in Fig. 10, the methyl oleate production increases linearly with the reduction in the catalyst diameter. As for methyl stearates, its production is constant in the diameter range of 2.3 mm-3.0 mm, and increases linearly from 1 mm to 1.8 mm. Since the trends of the FAME curves in the range of diameter evaluated are unique, it is difficult to determine the best composition, making its determination relies on the tests of oxidative stability and cold flow properties.

5. Conclusions

The mathematical model of upgrading biodiesel through the partial hydrogenation of polyunsaturated FAME in a trickle-bed reactor has been developed. The simulation result with the inlet temperature being 433 K, the reactor pressure being 611 kPa and the gas flowrate being 43 times higher than the liquid one shows that the process reached about 78% methyl linoleate conversion.

The formation of methyl stearate increases exponentially with temperature over the simulated temperature range, whereas the formation of methyl oleate has a maximum value at 430 K. At that temperature, methyl oleate and methyl stearate formed are 9578 grams/m^3 and 2656 grams/m^3, and the remaining methyl linoleate is 5633 grams/m^3 with the conversion being 68%.

Over the simulated pressure range, the highest value of the mass concentration of methyl oleate is 9296 grams/m^3, which takes place at 565 kPa. At the same pressure, the methyl stearate production is 3132 grams/m^3, whilst the remaining methyl linoleate is 5242 gram/m^3 with the conversion being 70%.

At the simulated catalyst diameter range, the methyl linoleate production increases linearly with the decrease in the catalyst size. The production of methyl stearate is constant in the diameter range of 2.3 mm-3.0 mm, and increases linearly from 1 mm to 1.8 mm.

Acknowledgement

We express our gratitude to the University of Indonesia, which funded this research through the scheme of Hibah Publikasi Artikel di Jurnal Internasional kuartil Q1 dan Q2 (Q1Q2) Tahun Anggaran 2019 No NKB-0032/UN2.R3.1/HKP.05.00/2019.

References

[1] D. Qi, L. Geng, H. Chen, Y. Bian, J. Liu, and X. Ren, "Combustion and performance evaluation of a diesel engine fueled with biodiesel produced from soybean crude oil," *Renew. Energy*, vol. 34, pp. 2706-2713, 2009.

[2] N. Ellis, F. Guan, T. Chen, and C. Poon, "Monitoring biodiesel production (transesterification) using in situ viscometer," *Chem. Eng. J.*, vol. 138, pp. 200–206, 2008.

[3] Y. H. Taufiq-Yap, H. V. Lee, R. Yunus, J. C. Juan, "Transesterification of non-edible Jatropha curcas oil to biodiesel using binary Ca–Mg mixed oxide catalyst: effect of stoichiometric composition," *Chem. Eng. J.*, vol. 178, pp. 342–347, 2011.

[4] M. Lapuerta, J. Sánchez-Valdepeñas, and E. Sukjit, "Effect of ambient humidity and hygroscopy on the lubricity of diesel fuels," *Wear*, vol. 309, pp. 200–207, 2014.

[5] J. W. Goodrum and D. P. Geller, "Influence of fatty acid methyl esters from hydroxylated vegetable oils on diesel fuel lubricity," *Bioresour. Technol.*, vol. 96, pp. 851–855, 2005.

[6] E. Sukjit, M. Tongroon, N. Chollacoop, Y. Yoshimura, P. Poapongsakorn, and K. D. Dearn, "Improvement of the tribological behaviour of palm biodiesel via partial hydrogenation of unsaturated fatty acid methyl esters," *Wear*, vol. 426–427, pp. 813–818, 2019.

[7] R. L. Mccormick, M. S. Graboski, T. L. Alleman, and A. M. Herring, "Impact of biodiesel source material and chemical structure on emissions of criteria pollutants from a heavy-duty engine," *Environ. Sci. Technol.*, vol. 35, pp. 1742-1747, 2001.

[8] J. Hwang, D. Qi, Y. Jung, and C. Bae, "Effect of injection parameters on the combustion and emission characteristics in a common-rail direct injection diesel engine fueled with waste cooking oil biodiesel," *Renew. Energy*, vol. 63, pp. 9-17, 2014.

[9] K. Wadumesthrige, J. C. Smith, J. R. Wilson, S. O. Salley, and K. Y. S. Ng, "Investigation of the Parameters Affecting the Cetane Number of Biodiesel," *J. Am. Oil Chem. Soc.*, vol. 85, no. 11, pp. 1073–1081, 2008.

[10] G. Knothe, "Some aspects of biodiesel oxidation stability," *Fuel Process. Technol.*, vol. 88, pp. 669–677, 2007.

[11] G. Knothe, "Dependence of biodiesel fuel properties on the structure of fatty acid alkyl esters," *Fuel Process. Technol.*, vol. 86, pp. 1059-1070, 2005.

[12] G. Knothe and R. O. Dunn, "A comprehensive evaluation of the melting points of fatty acids and esters determined by differential scanning calorimetry," *J. Am. Oil Chem. Soc.*, vol. 86, pp. 843–856, 2009.

[13] M. J. Ramos, C. M. Fernandez, A. Casas, L. Rodriguez, and A. Perez, "Influence of fatty acid composition of raw materials on biodiesel properties," *Bioresour. Technol.*, vol. 100, pp. 261-268, 2009.

[14] A. Bouriazos, S. Sotiriou, C. Vangelis, and G. Papadogianakis, "Catalytic conversions in green aqueous media: Part 4. Selective hydrogenation of polyunsaturated methyl esters of vegetable oils for upgrading biodiesel," *J. Organomet. Chem.*, vol. 696, pp. 327-337, 2010.

[15] F. Zaccheria, R. Psaro, N. Ravasio, and P. Bondioli, "Standardization of vegetable oils composition to be used as oleochemistry feedstock through a selective hydrogenation process," *Eur. J. Lipid Sci. Technol.*, vol. 114, no. 1, pp. 24-30, 2012.

[16] B. R. Moser, M. J. Haas, J. K. Winkler, M. A. Jackson, S. Z. Erhan, and G. R. List, "Evaluation of partially hydrogenated soybean oil methyl esters as biodiesel," *Eur. J. Lipid Sci. Technol.*, vol. 109, pp. 17–24, 2007.

[17] F. Zaccheria, R. Psaro, and N. Ravasio, "Selective hydrogenation of alternative oils: A useful tool for the production of biofuels," *Green Chem.*, vol. 11, pp. 462–465, 2009.

[18] N. Numwong, A. Luengnaruemitchai, N. Chollacoop, and Y. Yoshimura, "Effect of support acidic properties on sulfur tolerance of pd catalysts for partial hydrogenation of rapeseed oil-derived FAME," *Am. Oil Chem. Soc.*, vol. 89 pp. 2117-2120, 2012.

[19] J. Ni and F. C. Meunier, "Esterification of free fatty acids in sunflower oil over solid acid catalysts using batch and fixed bed-reactors," *Appl. Catal. A*, vol. 333 pp. 122–130, 2007.

[20] N. Shibasaki-Kitakawa, H. Honda, H. Kuribayashi, T. Toda, T. Fukumura, and T. Yonemoto, "Biodiesel production using anionic ion-exchange resin as heterogeneous catalyst," *Bioresour. Technol.*, vol. 98, pp. 416–421, 2007.

[21] F. S. Mederos, I. Elizalde, and J. Ancheyta, "Steady-state and dynamic reactor models for hydrotreatment of oil fractions: A review," *Cat. Rev. Sci. Eng.*, vol. 51, pp. 485–607, 2009.

[22] Y. Wang, J. Chen, and F. Larachi, "Modelling and simulation of trickle-bed reactors using computational fluid dynamics: A state-of-the-art review," *Can. J. Chem. Eng.*, vol. 91, pp. 136–180, 2013.
[23] F. S. Mederos and J. Ancheyta, "Mathematical modeling and simulation of hydrotreating reactors: Cocurrent versus countercurrent operations," *Appl. Catal. A*, vol. 332, pp. 8–21, 2007.
[24] N. Numwong, A. Luengnaruemitchai, N. Chollacoop, and Y. Yoshimura, "Partial hydrogenation of polyunsaturated fatty acid methyl esters over Pd/activated carbon: Effect of type of reactor," *Chem. Eng. J.*, vol. 210 pp. 173–181, 2012.
[25] D. H. Anderson and A. V. Sapre, "Trickle-bed reactor flow simulation," *AIChE J.*, vol. 37, no. 3, pp. 377-382, 1991.
[26] M. I. Cabrera and R. J. Grau, "Advanced concepts for the kinetic modeling of fatty acid methyl esters hydrogenation," *Int. J. Chem. React. Eng.*, vol. 6, Article A70, 2008.
[27] S. Goto and J. Smith, "Trickle-bed reactor performance: Holdup and mass transfer effects," *AIChE J.*, vol. 21, pp. 706-713, 1975.
[28] D. W. Van Krevelen and J. T. C. Krekels, "Rate of dissolution of solid substances," *Rec. Trau. Chim.*, vol. 67, pp. 512-520, 1948.
[29] M. J. Taulamet, N. J. Mariani, O. M. Martínez, and G. F. Barreto, "A critical review on heat transfer in trickle bed reactors," *Rev. Chem. Eng.*, vol. 31, no. 2, pp. 97-118, 2015.
[30] R. M. Propp, P. Colella, W. Y. Crutchfield, and M. S. Day, "A numerical model for trickle bed reactors," *J. Comput. Phys.*, vol. 165, pp. 311-333, 2000.
[31] A. E. Saez and R. G. Carbonell, "Hydrodynamic parameters for gas-liquid cocurrent flow in packed beds," *AIChE J.*, vol. 31, pp. 52-62, 1985.

Yuswan Muharam was born in Makassar, South Sulawesi, Indonesia in 1964. He received the B.S. degree in gas and petrochemical engineering from University of Indonesia, Depok, Indonesia in 2001, the M.S. degree in chemical engineering from University of Indonesia, Depok, Indonesia in 1995, and the Ph.D. degree in chemistry from Heidelberg University, Heidelberg, Germany in 2005.

From 1992 to 1995, he was a research assistant with Research Grant Programe of Pertamina-University of Indonesia, Indonesia, and from 2001 to 2005 he was a research assistant with the Interdisciplinary Center for Scientific Computing, Heidelberg University, Heidelberg, Germany. Since 1995, he has been a researcher and lecturer in the Department of Chemical Engineering, University of Indonesia, and since 2006 an associate professor with the same department. His research interests include modelling and simulation of chemical process system and renewable energy.

Taqi Aufa received the B.S. degree in chemical engineering from the University of Indonesia, Depok, Indonesia in 2018.

Since 2018, he has been worked for Pertagas, Indonesia as a process engineer. His undergraduate research topic is Modeling and Simulation of a Tricle-Bed Reactor for the Partial Hydrogenation of Polyunsaturated FAME to H-FAME.

Teguh Budi Santoso was born in Ngawi, East Java, Indonesia in 1988. He received the B.S. degree in chemical engineering from Sepuluh Nopember Institute of Technology (ITS), Surabaya, Indonesia in 2011, and the M.S. degree in chemical engineering from Universitas Indonesia, Depok, Indonesia in 2019.

Since 2019, he has been worked for P.T. Rekayasa Engineering, Indonesia as a process engineer. His master degree research topic is Experimental Study of Partial Hydrogenation of Polyunsaturated FAME to H-FAME in a Tricle-Bed Reactor.